JACS
JOURNAL OF THE AMERICAN CHEMICAL SOCIETY
Article
pubs.acs.org/JACS

Mesomorphic [2]Rotaxanes: Sheltering Ionic Cores with Interlocking Components

Natalie D. Suhan, Stephen J. Loeb,* and S. Holger Eichhorn*

Department of Chemistry and Biochemistry, University of Windsor, Windsor, Ontario, N9B 3P4, Canada

Supporting Information

ABSTRACT: Two types of liquid crystalline [2]rotaxanes based on a conventional tetracatenar motif (a rod-shaped molecule with two side chains at each end) have been prepared. Dicationic compounds with ester stoppers and tetracationic materials with pyridinium stoppers are compared to each other and their dumbbell shaped analogs. Since the ionic core contributes about 70% to the overall length and molecular weight of the molecules, sheltering the ionic cores with an interlocked neutral macrocycle has considerable effect on the mesomorphism and thermal stability of the materials. The influence of the sheltering macrocycle, the numbers of charges on the core and the size and nature of the side chains (aliphatic vs siloxane) were probed. [2]Rotaxanes with linear side chains and minimum ratios of chain-to-core volumes of about 0.35 and 0.30 for tetra- and dicationic compounds, respectively, display smectic liquid crystal phases. Larger ratios increase the temperature range of the smectic A phases beyond the decomposition temperatures; a disadvantage for processing because no stable isotropic liquid phase is available. The change from tetra- to dicationic [2]rotaxanes increased not only the fluidity of their smectic A phases but also their thermal and chemical stability. Branched side chains (2-hexyldecyl) disfavor the formation of lamellar mesophases and, instead, induce higher ordered soft crystal phases. No liquid crystal phases but soft crystal phases are observed for the analogous di- and tetracationic compounds without an ion sheltering interlocked macrocycle (dumbbells).

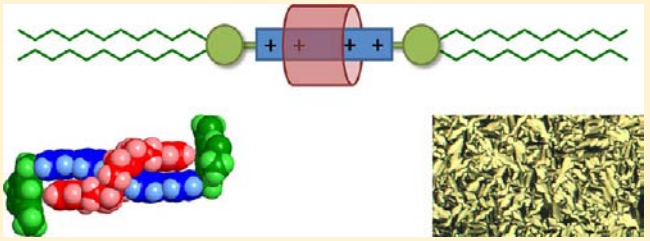

INTRODUCTION

Over the past 20 years, the concept of mesomorphism has been extended well beyond the classical structural motifs of liquid crystals (LCs). Judicious application of shape anisotropy, directed molecular interactions, self-assembly, and microphase segregation have converted typical nonmesogens, such as C_{60}[1] and other molecules with low or unfavorable aspect ratios, including ionic molecules, into compounds that display mesophases over a wide range of temperatures.[2]

Mechanically interlocked molecules (MIMs), such as [2]-rotaxanes, are interesting candidates for inclusion into mesogens due to the complex nature of their component building blocks, their size, and often ionic character.[3] It was only recently that the first liquid crystalline [2]rotaxane and [2]catenane were reported by Kato in collaborations with Stoddart[4] and Sauvage,[5] respectively, and the first example of a mesophase forming polyrotaxane reported by Kidowaki et al.[6] The feasibility of molecular switching in a mesophase was also clearly demonstrated by Kato and Stoddart who showed that a bistable [2]rotaxane could be electrochemically switched between two different molecular states in a liquid crystal phase.[7] These initial studies were undoubtedly motivated by the intriguing prospect of preparing self-organizing molecular switches since it may eventually be possible to amplify the molecular switching process in a mesophase by cooperative motion, thereby producing a directed (anisotropic) macroscopic response. Stimuli responsive materials are of both academic and commercial interest,[8] and the idea of molecular switches based on liquid crystalline rotaxanes represents a new approach to these types of materials.

Despite the impressive syntheses of these first examples of liquid crystalline materials containing MIMs, no predictive knowledge has been generated that would allow for the rational design of liquid crystalline interlocked molecules. In fact, very little is known about the mesomorphism of ionic liquid crystals that have multiple charges on a rigid rod core, and completely unexplored is the effect of an interlocked macrocyclic ring on mesomorphism in general. An investigation of these structure–property relationships for ionic liquid crystalline [2]rotaxanes is also of fundamental interest because it adds to the body of work that has been produced on thermotropic ionic liquid crystals.[9] All reported thermotropic ionic liquid crystals with multiple charges located on a rigid-rod core are based on doubly charged viologen salts,[10] except for single reports on dimeric 2,4,6-triarylpyrylium[11] and bis(benzimidazolium)[12] derivatives.

Presented herein is the synthesis and characterization of two classes of liquid crystalline ionic [2]rotaxanes and their dumbbell analogs (stoppered axles without a macrocycle component) based on a conventional tetracatenar motif. In this design, the charged core contributes about 70% to the overall length and molecular weight of the entire molecule.

Received: October 1, 2012
Published: December 10, 2012

   dx.doi.org/10.1021/ja309558p | J. Am. Chem. Soc. 2013, 135, 400–408

Consequently, structural changes to the core considerably affect the mesomorphism of the material. Of the investigated structural variations: (i) addition of the neutral macrocycle (comparison of dumbbells and [2]rotaxanes); (ii) two versus four charges (positive) on the core, (iii) size, and (iv) nature of the side chains; the addition of the neutral macrocycle is most effective in the introduction of mesomorphism. This result is attributed to a sheltering of the charges on the core by the neutral macrocycle that significantly reduces intermolecular ionic interactions. Thus, [2]rotaxanes based on a small molecule design that form stable liquid crystal and isotropic liquid phases are obtained for the first time. Although not investigated here, this new design provides a blueprint for the preparation of analogous switchable [2]rotaxanes[3o,s] that might be expected to display a macroscopic response if MIM switching were to be achieved in a liquid crystalline phase.

RESULTS AND DISCUSSION

Design. Thermotropic ionic liquid crystals form mesophases when heated above their melting temperature and, in contrast to lyotropic ionic liquid crystals, do not require the presence of a solvent. The majority of known thermotropic ionic liquid crystals consist of singly charged surfactant-like molecules, and their self-organization is primarily controlled by amphiphilic interactions that often promote both thermotropic and lyotropic mesomorphism. More recently, structural features of amphiphilic ionic liquid crystals were combined with mesogenic rod-shaped rigid cores of conventional calamitic liquid crystals, but in many of these approaches, the charged units were attached via flexible spacers and were not part of the rigid core.[9]

Only a few examples of thermotropic ionic liquid crystals consisting of a charged rigid-rod core centered between side chains have been reported.[11] Examples are the thermotropic ionic liquid crystals based on rigid-rod metal complexes developed by Bruce[13] and others,[14] doubly charged viologens,[10] and a range of imidazolium containing rigid-rod ionic liquid crystals recently studied by Swager[15] and others.[12] The mesomorphism of all these compounds was altered by a change of anions and attached side chains to optimize amphiphilic interactions and excluded volume effects.

The alteration of the size and type of side chains is employed here for the creation of LC [2]rotaxanes. Also varied is the core charge between 4+ in the ionic core based on two viologen-like 4,4′-bipyridinium groups linked by an ethylene chain (Scheme 1) and 2+ in the analogous 4-phenyl-pyridinium derivative (Scheme 2). All [2]rotaxanes have two side chains attached to each aromatic end group (tetracatenar motive), as this was predicted to provide the best match between the packing volumes of the cores and the side chains for the formation of lamellar mesophases. A branched 2-hexyldecyl and a siloxane chain were tested in addition to linear alkyl chains of various lengths, as they have been shown to promote tilted lamellar mesophases such as SmC.[16] Most importantly, all these compounds can be prepared with and without a dibenzo[24]-crown-8 ether (**DB24C8**) macrocycle that wraps around the majority of the pyridinium core charges allowing direct comparison of the "naked" charged species (dumbbells) to the analogous [2]rotaxanes as depicted in Figure 1. The use of an uncharged macrocycle and a charged core, in contrast to the charged macrocycle employed by Stoddard and Kato,[4] is also expected to promote the formation of liquid crystal phases by sheltering the ionic cores and reducing strong ionic interactions between the di- or tetracationic [2]rotaxane molecules.

Scheme 1. Synthesis of [2]Rotaxanes $R1^{4+}$–$R16b^{4+}$ Containing DB24C8 as the Macrocycle and Their Corresponding Dumbbells $D1^{4+}$–$D16b^{4+}$ without the Macrocycle[a]

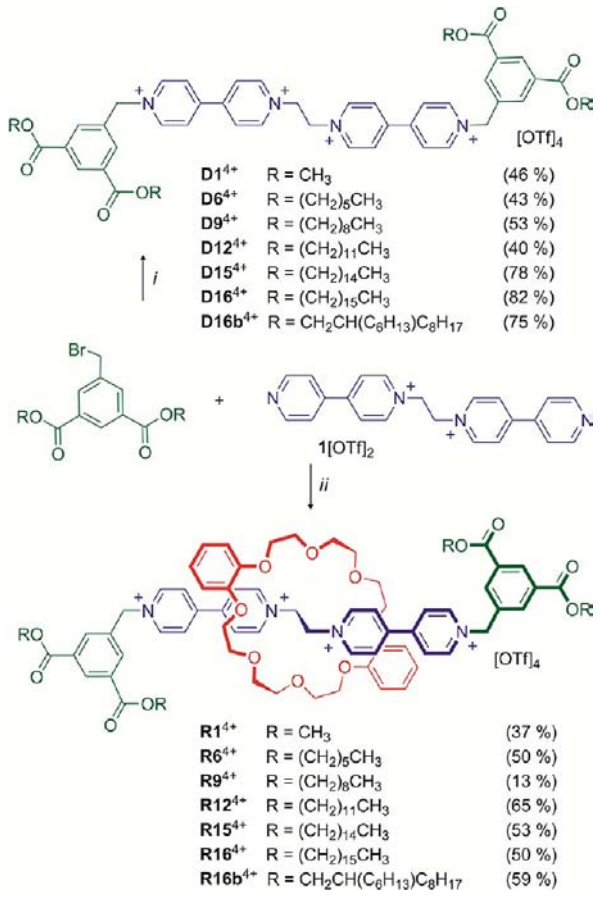

[a](i) $CH_3NO_2/CHCl_3$ 60 °C, 3 days; (ii) 8 equiv **DB24C8**, $CH_3NO_2/CHCl_3$ 50 °C, μW 200 W, 5h followed by NaOTf(aq) and a further 50 °C, μW 200 W, 5–15 h. Reported yields are isolated after multiple runs of column chromatography (see SI for details).

Scheme 2. Synthesis of [2]Rotaxanes $R1^{2+}$, $R12^{2+}$, and RSi^{2+} containing DB24C8 as the Macrocycle and the Dumbbell $D12^{2+}$[a]

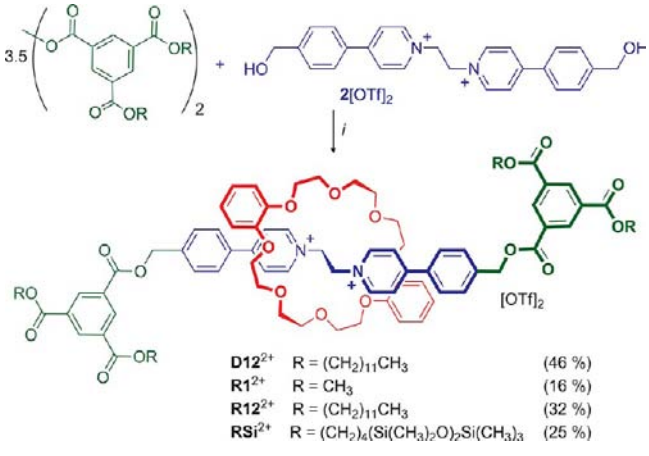

[a](i) 7:3 $CHCl_3/CH_3CN$, Bu_3P cat., RT, 3 h; 5 equiv **DB24C8** for [2]rotaxanes, no crown for the dumbbell. Reported yields are isolated after multiple runs of column chromatography (see SI for details).

dx.doi.org/10.1021/ja309558p | J. Am. Chem. Soc. 2013, 135, 400–408

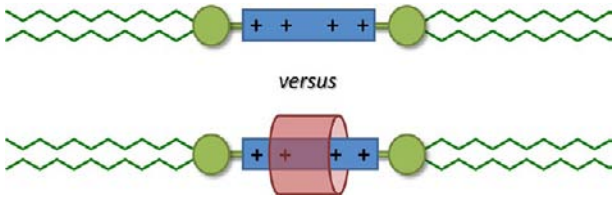

Figure 1. Cartoon depiction of dumbbell (top) and [2]rotaxane (bottom) featuring a tetracatenar structural motif designed to induce mesomorphism.

Synthesis. The 4+ charged [2]rotaxanes $\mathbf{R1}^{4+}$–$\mathbf{R16b}^{4+}$ and their corresponding dumbbells $\mathbf{D1}^{4+}$–$\mathbf{D16b}^{4+}$ were prepared by alkylation of the terminal pyridine groups of axle 1,2-bis(4,4′-bipyridinium)ethane, $\mathbf{1}[OTf]_2$ with the appropriate 3,5-diester-substituted benzylbromide, in the presence (rotaxane) or absence (dumbbell) of the macrocycle **DB24C8**, as outlined in Scheme 1.[17]

The preparation of the dumbbells is straightforward, while preparation and purification of the [2]rotaxanes is more challenging. Traditionally, [2]rotaxane formation with this templating motif involves prolonged reaction at room temperature until all terminal pyridine groups are alkylated,[17] ranging from days to weeks with reaction times increased for this study due to extreme solubility differences between the ionic axles and aliphatic stoppers. Efforts to decrease reaction times by heating were thwarted by a marked decrease in pseudorotaxane formation and correspondingly poorer yields. To decrease reaction times and increase product yields, microwave irradiation was employed.[17a] Temperatures as high as 50 °C yielded nearly complete [2]rotaxane formation (>80%, ^{1}H NMR) in 5–15 h (SI).

As outlined in Scheme 2, dumbbell $\mathbf{D12}^{2+}$ and [2]rotaxanes ($\mathbf{R1}^{2+}$, $\mathbf{R12}^{2+}$, and $\mathbf{RSi}^{2+}$) were synthesized by ester formation using conditions reported by Takata et al.[18] This system offered a significant synthetic improvement as [2]rotaxane formation was complete in ca. 3 h, with no formation of the usual dumbbell side products. Purification was accomplished by multiple runs of column chromatography employing fully end-capped RP-C_{18} silica gel and methanol as the eluent. For both 4+ and 2+ charged systems, the isolated yield depended upon the effectiveness of the chromatography and the number of runs required to achieve sufficient purity for LC experiments.

Single-Crystal X-ray Structures of Model Compounds. [2]Rotaxanes $\mathbf{R1}^{4+}$ and $\mathbf{R1}^{2+}$, containing R = Me groups, were prepared as compounds that would be expected to be crystalline versions of the LC [2]rotaxanes in these series; as designed, they do not melt before they start to decompose at temperatures >200 and 260 °C, respectively. Unfortunately, single crystals of $\mathbf{R1}^{2+}$ were too small for X-ray analysis, however suitably sized crystals of the closely related derivative $\mathbf{MR1}^{2+}$ (Me groups in place of COOMe groups) could be grown. Thus, single-crystal X-ray structures were obtained for $\mathbf{R1}[CF_3SO_3]_4$ and the derivative $\mathbf{MR1}[BF_4]_2$.

Importantly these structures, as depicted in Figure 2, provide an idea of the overall arrangement of the major structural features in these compounds, for example, the position of the anions relative to the cationic axle/wheel core and the conformation of the stopper groups with respect to the rotaxane core. Compounds with longer chains either do not form single crystals of sufficient quality or are not crystalline. It is assumed for the purpose of estimating molecular dimension (see Table 1) that the ionic cores of the compounds with longer chains are similar to those observed for the X-ray structures of these model compounds.

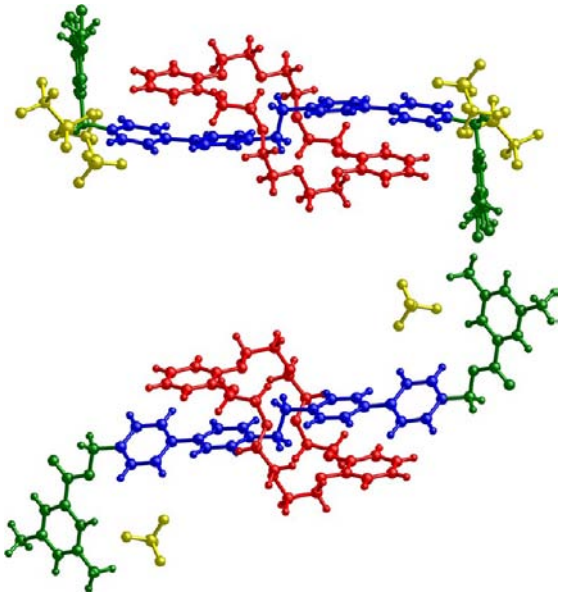

Figure 2. X-ray crystal structures of $\mathbf{R1}^{4+}$ (top) and $\mathbf{MR1}^{2+}$ (bottom) showing the relative positioning of the axle (blue), macrocycle (red), stoppering groups (green), and anions (gold) in the solid state.

Both, $\mathbf{R1}^{4+}$ and $\mathbf{MR1}^{2+}$ show a typical S-shaped conformation for the macrocycle **DB24C8**, and the stopper groups are oriented in a zigzag shape, i.e., up and down relative to the rotaxane plane with the anions positioned close to the ends of the core.[19] One of the main differences in overall structure is that for $\mathbf{R1}^{4+}$ the benzylic stopper groups are almost orthogonal to the core axis, while for $\mathbf{MR1}^{2+}$ the benzoic ester stopper groups are twisted outward at an angle of about 120° to the core.[17a]

The basic shape of the molecular components and the positioning of the cations and anions might be expected to persist throughout a series of related compounds in which only changes to peripheral R-groups have been made. However, the lowest energy conformation of the molecule in a mesophase would likely differ greatly from that observed in the crystalline phase and may be altered significantly by the exchange of methyl groups for longer and more flexible alkyl chains. Nevertheless, the differences in observed mesomorphism for $\mathbf{R12}^{4+}$and $\mathbf{R12}^{2+}$ (*vide infra*) are consistent with the basic structural features observed for the [2]rotaxanes in the crystal structures of model compounds $\mathbf{R1}^{4+}$and $\mathbf{MR1}^{2+}$, justifying the use of their crystallographic parameters to estimate the molecular dimensions summarized in Table 1.

Estimation of Molecular Dimensions. Space filling calculations were performed for all dumbbells and [2]rotaxanes to compare molecular dimensions with layer spacings and other packing distances obtained by PXRD (see Table 1). Core volumes were calculated as cylindrical excluded volumes and imply a free rotation of the molecules over their long axis, as is the case in smectic liquid crystal phases. The dimensions of the 2+ and 4+ charged cores are based on their conformations in the crystal structures of model compounds $\mathbf{R1}^{4+}$and $\mathbf{MR1}^{2+}$ and include all anions, the aromatic parts of the stopper groups, and for [2]rotaxanes, the crown ether macrocycle. Core lengths of 2+ and 4+ charged cations differ (29.8 and 27.4 Å, respectively), while their average diameters (average of

dx.doi.org/10.1021/ja309558p | J. Am. Chem. Soc. 2013, 135, 400–408

Table 1. Estimated Molecular Dimensions of Dumbbells and [2]Rotaxanes, Inclusive of $CF_3SO_3^-$ Anions

	core dimensions[a]			chain dimensions[b]		totals[c]		experimental values	
compd	L_{core} (Å)	W_{core} (Å)	V_{core} (Å^3)	V_{chains} (Å^3)	L_{chains} (Å)	L_{max} (Å)	L_{tot} (Å)	d-spacing (Å), (T (°C), phase)[d]	AR[e]
D6^{4+}	27.4	8.1	1350	440	8.5	42.6	35.9	32.8 (30, SC)	4.4
D9^{4+}	27.4	8.1	1350	640	12.4	49.1	39.8	45.0 (30, SC1), 38.8 (100, SC2)	4.9
D12^{4+}	27.4	8.1	1350	850	16.5	55.6	43.9	45.0 (25, SC1), 45.5 (90, SC2)	5.4
D16^{4+}	27.4	8.1	1350	1120	21.7	64.2	49.1	48.9 (25, $SC7_L$), 50.3 (130, $SC5_L$)	6.1
D16b^{4+}	27.4	8.1	1350	1150	22.3	51.7	49.6	37.3 (25, SC)	6.1
R6^{4+}	27.4	10.6	2400	440	5.0	42.6	32.4	30.5 (25, SC)	3.1
R9^{4+}	27.4	10.6	2400	640	7.3	49.1	34.7	35.9 (30, SC)	3.3
R12^{4+}	27.4	10.6	2400	850	9.6	55.6	37.0	39.6 (100, SmA), 38.5 (150, SmA)	3.5
R16^{4+}	27.4	10.6	2400	1120	12.7	64.2	40.1	44.6 (25, SmX1), 42.9 (100, SmA)	3.8
R16b^{4+}	27.4	10.6	2400	1150	13.0	51.7	40.4	33.7 (25, SC1), 32.8 (130, SC2)	3.8
D12^{2+}	29.8	8.1	1536	850	16.5	54.9	46.3	39.3 (30, SC1), 40.8 (140, SC2)	5.7
R12^{2+}	29.8	10.6	2630	850	9.6	54.9	39.4	39.8 (25, SmA)	3.7
RSi^{2+}	29.8	10.6	2630	1200	13.6	53.8	43.4	42.2 (25, SmA)	4.1

[a]From single-crystal X-ray structures of **R1**$^{4+}$ and **MR1**$^{2+}$. $V_{core} = \pi(W_{core}/2)^2 L_{core}$. [b]Established values for the molten state from ref 20. $L_{chain} = V_{chain}/\pi(W_{chain}/2)^2$ and assuming $W_{core} = W_{chain}$. [c]From AM1 calculations on models with extended chains where X-ray structures of **R1**$^{4+}$ and **MR1**$^{2+}$ were used as the basis of the model. $L_{tot} = L_{core} + L_{chain}$. [d]Smallest angle reflection measured by PXRD at given temperature. [e]Aspect ratio L_{tot}/W_{core}.

maximum and minimum core width) are identical but differ between dumbbells (8.1 Å) and [2]rotaxanes (10.6 Å). The overall length of the cylindrical space the molecule occupies is calculated based on the assumption that both core and side chains fill a cylindrical (excluded) volume of the same diameter. A cylindrical volume occupied by side chains is then calculated based on the established packing volumes of hydrocarbon and siloxane groups in their isotropic liquid phases.[20] Consequently, the calculated packing dimensions are estimations of the minimum layer spacing and in-plane intermolecular distances for a uniaxial lamellar liquid crystalline phase (e.g., SmA) and are independent of the degree of interdigitation. Estimated molecular lengths for all *trans* extended side chains (L_{max}) are also provided in Table 1 for comparison.

Thermal stability. Thermal gravimetric analysis (TGA) of all [2]rotaxanes and dumbbells was performed to probe their thermal stability and the presence of any residual volatile compounds (Table S2). Samples dried in vacuum below their melting temperatures show a small weight loss of up to 0.5% between 50 and 100 °C, which is attributed to the loss of acetonitrile that is also present in the single crystals of **R1**$^{4+}$ and other related [2]rotaxanes. No further measurable weight loss occurs until the onset of decomposition at temperatures >150 °C. Decomposition temperatures are estimated not only based on weight loss in TGA but also degradation observed by differential scanning calorimetry (DSC) and NMR measurements of heated samples. Thermal stability values measured by TGA at a heating rate of 2 °C/min under He(g) best agree with the values obtained by DSC and NMR when the limit of thermal stability is defined as the temperature at which 0.3% of weight loss has occurred, rather than the extrapolated onset, a common procedure for polymers.[21]

All dumbbells reach a weight loss of 0.3% at about 170 °C, whereas their analogous 4+ and 2+ charged [2]rotaxanes, except for **R4Si**$^{2+}$, do not reach the 0.3% marker <190 and 250 °C, respectively (Table S2). Clearly, complexation with a macrocycle increases the thermal stability of the axle and is more effective for the 2+ charged compounds. The stabilization can be reasoned with a better delocalization of the positive charges on the axle due to charge-transfer interactions between the electron-deficient pyridinium groups and the electron-rich catechol groups of the crown. Surprisingly, [2]rotaxane **RSi**$^{2+}$ is the least stable of the five [2]rotaxanes because it already reaches the 0.3% marker at 165 °C, but this is likely due to decomposition of the siloxane groups (*vide infra*).

All compounds decompose in several distinct weight loss steps (Figure 3). The % weight loss of the first step correlates

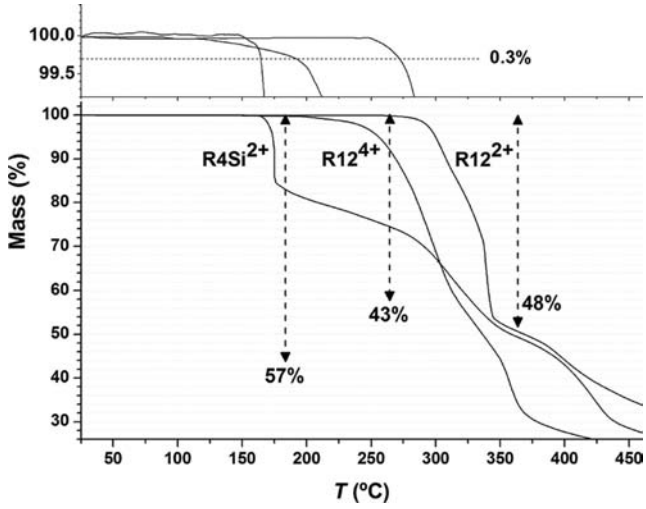

Figure 3. TGA curves for the 4+ charged [2]rotaxane **R12**$^{4+}$ and 2+ charged [2]rotaxanes **R12**$^{2+}$ and **RSi**$^{2+}$ obtained at a heating rate of 2 °C/min under He(g). Double-headed arrows show the calculated weight loss for the removal of both stopper groups. The onset of weight loss is defined as the temperature at which 0.3% weight loss has occurred and is marked in the enlarged view at the top of the graph. All samples were preheated in vacuum to remove remaining solvent.

with mass contributions from the benzylic and ester stopper groups in all cases but **R4Si**$^{2+}$ (Table S2). TGA of **R1**$^{4+}$ coupled with mass spectrometric analysis of the evolved gas supports thermal cleavage of the C−N$^+$ bond as a high concentration of fragment ion peaks characteristic for the benzylic stopper was detected during the first weight loss event. Consequently, the thermal stability of the 4+ charged compounds is limited by the C−N$^+$ bond between the pyridinium and benzylic groups and the stability of the 2+ charged compounds by the benzoate esters.

dx.doi.org/10.1021/ja309558p | J. Am. Chem. Soc. 2013, 135, 400−408

Similar decomposition temperatures have been reported for other pyridinium compounds and benzyl benzoates.[22] $\mathbf{RSi}^{2+}$ shows an unexpectedly low thermal decomposition temperature of only 175 °C, 95 °C below the thermal decomposition of $\mathbf{R12}^{2+}$. This difference is attributed to an initial decomposition of the siloxane chains since this represents the only structural difference between $\mathbf{RSi}^{2+}$ and $\mathbf{R12}^{2+}$. The combined % weight losses of the first and second steps account for two ester stopper groups suggesting that ester cleavage of the benzyl benzoate constitutes the second weight loss − the onset temperature of about 260 °C is similar to $\mathbf{R12}^{2+}$.

Mesomorphism: General Observations. All [2]-rotaxanes and dumbbells, except the crystalline compounds $\mathbf{R1}^{4+}$ and $\mathbf{D1}^{4+}$, are soft birefringent materials at room temperature. The temperature-dependent (thermotropic) mesomorphism of these materials was studied by polarized optical microscopy (POM), differential scanning calorimetry (DSC), and variable temperature X-ray diffraction (vt-PXRD) (see SI for details). Many of the phase transitions occur slowly because the mesophases of these high molecular weight ionic compounds have high viscosity. To circumvent measurements on kinetically trapped rather than thermodynamically stable phases, POM images and XRD patterns were monitored at specific temperatures for up to several hours to identify nonequilibrium states by changes that occurred over time.

Many of the [2]rotaxanes and dumbbells displayed rich poly(meso)morphism, but only compounds $\mathbf{R12}^{4+}$, $\mathbf{R16}^{4+}$, $\mathbf{R12}^{2+}$, and $\mathbf{RSi}^{2+}$ formed mesophases that are liquid crystal phases. All other phases were categorized, based on their diffraction patterns, as soft-crystal phases (SC) of unknown structure or lamellar structure (SC_L) (Figure 4). Phases were

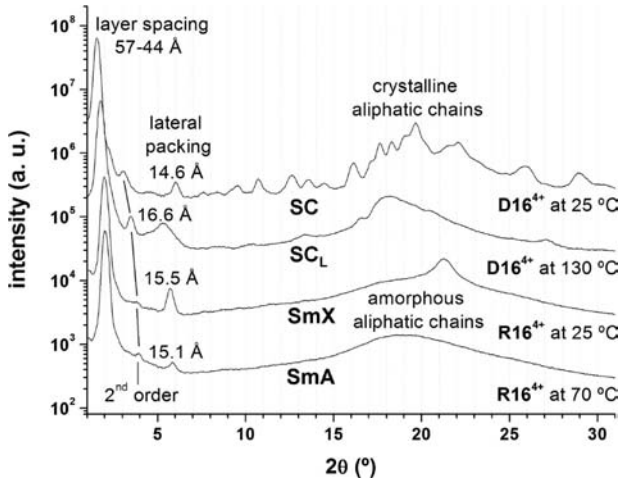

Figure 4. Example XRD patterns of the (lamellar) soft crystal phase (SC) and lamellar soft crystal phases (SC_L) of $\mathbf{D16}^{4+}$ and the SmX and SmA liquid crystal phases of $\mathbf{R16}^{4+}$.

categorized as SC phases when their diffraction patterns contained several additional reflections to what is observed for liquid crystal phases and could not be indexed based on plane groups. However, the degree of crystalline order varies widely between different SC phases, and differences are particularly obvious in the angle range of 15−22° 2-θ (d-spacings of 6 − 4 Å) that is indicative of the degree of crystallinity of the aliphatic side chains. A crystalline state of the aliphatic side chains generates sharp reflections and an amorphous state a broad diffuse reflection (halo).

The diffraction pattern of the SC phase of $\mathbf{D16}^{4+}$ is shown as an example in Figure 4. The softness of these crystal phases was confirmed by POM studies that showed the crystallites deform like viscous fluids under pressure (Figure 5). Crystallites were obtained only by precipitation from solution and did not form in the bulk phase upon cooling from higher temperature phases.

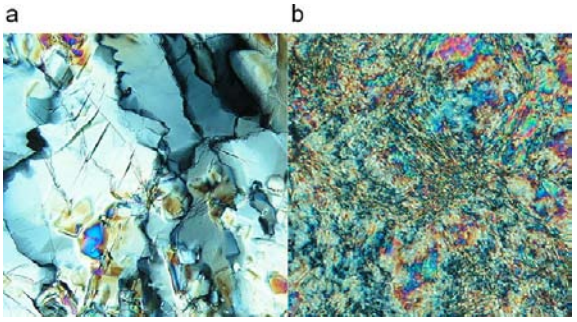

Figure 5. POM photomicrographs (crossed polarizers, 25 °C) of $\mathbf{D6}^{4+}$. (a) As crystallites precipitated from solution. (b) The same area after pressure was applied to the cover slide to generate a birefringent viscous fluid-like appearance.

Many of the SC phases show a single intense small angle reflection at a d-spacing close to the calculated layer spacing for a SmA-type packing of the molecules (Table 1), but a simple lamellar structure can be excluded because of additional small angle reflections. Lamellar structures (SC_L), however, are proposed for SC phases of $\mathbf{D16}^{4+}$ (Figure 4) and $\mathbf{R12}^{4+}$ because their diffraction patterns contain a second-order reflection of the layer spacing as the only other reflection below 5° 2-θ.

All our attempts of obtaining good quality 2D diffraction patterns of well-aligned SC phases failed, and no attempt was made to index the reflections based solely on 1D diffraction patterns. However, the diffraction patterns did not agree with patterns of crystal smectic B, E, and T phases that have been regularly observed in ionic smectic liquid crystals. This is not surprising because the formation of crystal smectic B, E, and T phases is usually driven by ordering of ionic head groups within bilayers.[23] Bilayer formation is unlikely to occur in the dumbbells and [2]rotaxanes presented herein, since the charged groups are associated with the rod-shaped core in the center of the molecules. A bilayer packing would only be possible if the cores form dimers and the side chains are oriented to both sides orthogonally to the cores, similar to what has been proposed for disc-shaped mesogens with polyionic cores.[24] However, the expected layer spacings of bilayers are much smaller than the measured spacings because the four side chains on each side would fully interdigitate with the side chains of the next layer to fill the available space.

A strong reflection at spacings between 14.5 and 17 Å observed in the diffraction patterns of all phases of 4+ charged dumbbells and [2]rotaxanes (Figure 4) must originate from the lateral packing of the molecules, as it is independent of the molecular length and was the only consistent indication of partial in-plane order. The d-spacing is about twice the average diameter of the dumbbells and [2]rotaxanes including all anions of about 8−10 Å and likely originates from short-range, ordered packing of the anions. A comparison with the single crystal structure of $\mathbf{R1}^{4+}$ confirmed that the packing distances of the

dx.doi.org/10.1021/ja309558p | J. Am. Chem. Soc. 2013, 135, 400−408

anions along the *c*-axis (10.7 and 9.8 Å) are of this order (Figure 2).

Mesomorphism: 4+ Charged Dumbbells. Characterization of the mesomorphism of the 4+ charged dumbbells was mainly based on DSC and XRD studies because defect textures observed by POM were unspecific, except for focal-conic-type textures displayed by $\mathbf{D12}^{4+}$. Dumbbells $\mathbf{D6}^{4+}$–$\mathbf{D16b}^{4+}$ all form soft-crystal phases that decrease in degree of crystallinty with increasing length of side chains, but no liquid crystalline phases are formed (Figure 6).

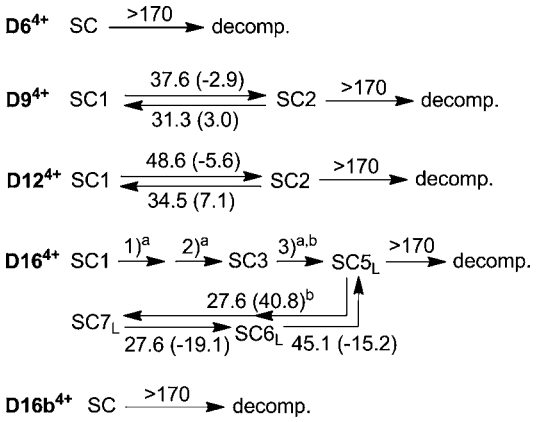

Figure 6. Phase transition temperatures in °C and enthalpies in kJ/mol of 4+ charged dumbbells based on POM, DSC, and XRD analysis (SC = soft crystal phase; SC_L = lamellar SC phase; numbers (e.g., SC1, SC2) designate different phases of the same category for each compound). (a) Transition temperatures (enthalpies): (1) 43.7(−1.5), (2) 69.8(−5.8), (3) 113.1(−21.3); and (b) two overlapping transitions.

Compound $\mathbf{D16}^{4+}$ is the only dumbbell derivative that displays SC phases of lamellar structures, while its analogous dumbbell $\mathbf{D16b}^{4+}$ with branched side chains does not, possibly because the increased lateral packing volume of the branched side chains disfavors a lamellar structure. A similar change from smectic to columnar and cubic mesophases has been reported for catenar liquid crystals when the lateral packing volume of the side chains is increased.[25]

Mesomorphism: 4+ Charged [2]Rotaxanes. The 4+ charged [2]rotaxanes $\mathbf{R6}^{4+}$–$\mathbf{R16}^{4+}$ are less crystalline than their parent dumbbells and clear into isotropic liquid phases below their decomposition temperature of about 190 °C, except for $\mathbf{R16}^{4+}$ (Figure 7). [2]Rotaxanes $\mathbf{R6}^{4+}$ and $\mathbf{R9}^{4+}$ form highly viscous SC phases that clear into isotropic liquids at 81 and 118 °C, respectively. Attachment of longer aliphatic chains in [2]rotaxanes $\mathbf{R12}^{4+}$ and $\mathbf{R16}^{4+}$ expectedly promotes lamellar packing order and introduces liquid crystal phases. Compound $\mathbf{R12}^{4+}$ forms a lamellar SC phase when precipitated from solution but irreversibly converts to a SmA phase at 53 °C based on POM, DSC, and XRD (Figure 8). The SmA phase reversibly clears into an isotropic liquid at 137 °C.

The presence of first- and second-order reflections of the layer structure in the diffraction patterns of $\mathbf{R12}^{4+}$ indicates a high periodicity of the layer spacing (Figure 8). A broad reflection at 15.5 Å is assigned to the packing of the anions within layers discussed above, and the diffuse reflection at 4.5 Å is characteristic for an amorphous state of the aliphatic side chains. The measured *d*-spacing of about 39 Å is 2 Å larger than the estimated minimum layer spacing of 37 Å but 16 Å shorter

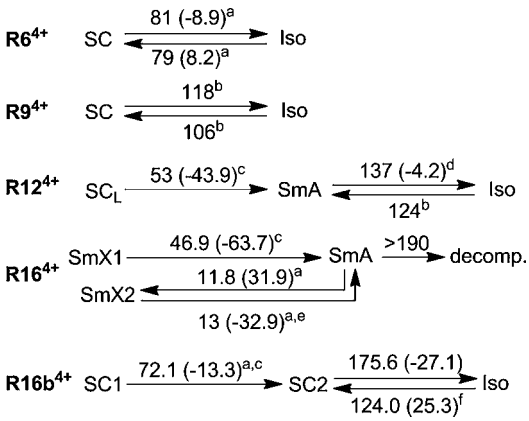

Figure 7. Phase transition temperatures in °C and enthalpies in kJ/mol of 4+ charged [2]rotaxanes based on POM, DSC, and XRD analysis (SC = soft crystal phase; SC_L = lamellar SC phase; SmX = unknown smetic liquid crystal phases; SmA = smectic A liquid crystal phase; Iso = isotropic liquid phase). (a) Broad transition; (b) determined by POM (not observed by DSC); (c) observed only in the first heating run of a compound precipitated from solution;(d) observed by DSC only in the first heating run but observed by POM in subsequent heating runs; (e) this transition consists of one large and two small overlapping transitions; (f) sample remains isotropic on cooling and forms the SC phase upon heating at 124 °C.

than the spacing for an expanded molecule (Table 1). XRD patterns of the initial SC_L phase are almost identical with the patterns of the SmA phase, except for some additional weak and broad reflections that indicate a higher degree of order than in the SmA phase. These small changes in the diffraction patterns are contrasted by a large enthalpy of 40 kJ/mol for the SC_L to SmA transition. A possible explanation for the large enthalpy is the concomitant loss of solvent molecules at this phase transition, which also explains its irreversibility.

The assignment of a SmA phase is also supported by the observation of characteristic fan-shaped textures of focal domains upon cooling from the isotropic liquid in cells with planar alignment layer and large pseudo-isotropic areas in cells treated with cetyl-trimethylammonium bromide for vertical (homeotropic) alignment (Figure 8). The latter observation confirms the optically uniaxial character of the phase. 2D XRD studies of a mechanically aligned fiber of $\mathbf{R12}^{4+}$ in its SmA phase confirm the expected alignment of the smectic layers parallel to the fiber axis (Figure 8). Unfortunately, the reflection at 15.5 Å and the halo of the amorphous side chains are not observed in the 2D pattern because of too low intensity. Both reflections are expected to be orthogonal to the layer reflections. All observations but the fan-shaped defect texture would also agree with a SmB phase, and in fact, short-range in-plane positional correlations indicated by the reflection at 15.5 Å are typically observed in SmB and not in SmA phases. Consequently, the presence of SmB phases is excluded solely based on the absence of mosaic defect textures.[26]

Attachment of longer C_{16} aliphatic chains in $\mathbf{R16}^{4+}$ stabilizes smectic mesomorphism and increases the fluidity of the phases. $\mathbf{R16}^{4+}$ displays two unknown smectic phases SmX1 and SmX2 at low temperature and a SmA phase at higher temperature that is stable beyond the onset of decomposition at 190 °C. Diffraction patterns of the SmA phases of $\mathbf{R16}^{4+}$ and $\mathbf{R12}^{4+}$ are virtually identical, except for the larger layer spacing of 43 Å for $\mathbf{R16}^{4+}$ that is 3 Å larger than the estimated minimum spacing of 40 Å (Table 1).

dx.doi.org/10.1021/ja309558p | J. Am. Chem. Soc. 2013, 135, 400−408

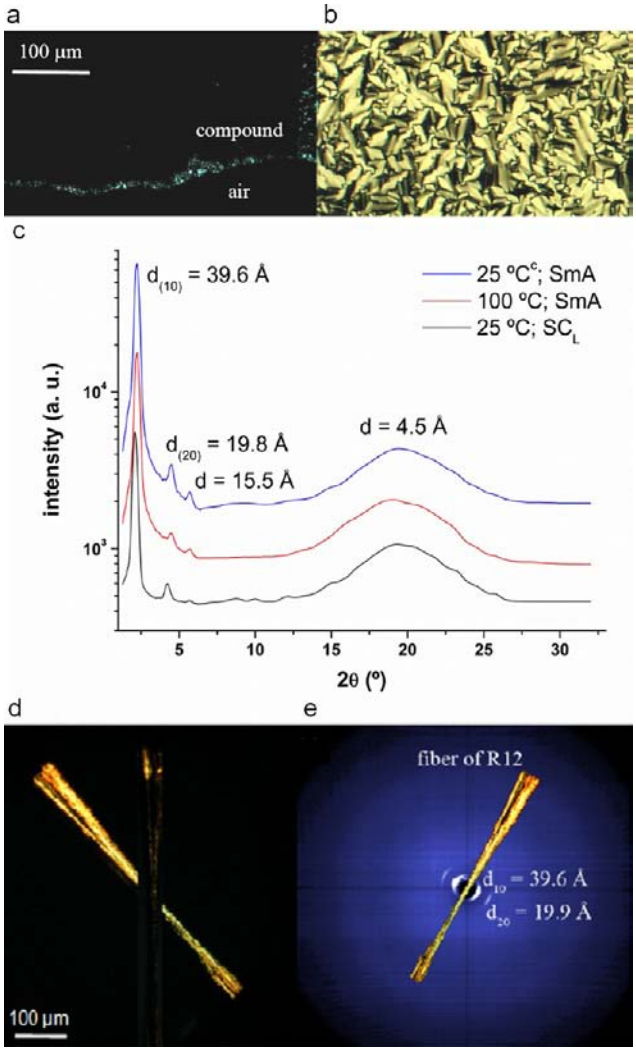

Figure 8. Optical micrographs of $\mathbf{R12}^{4+}$ in (a) a liquid crystal cell coated with cetyl-trimethylammonium bromide for vertical (homeotropic) alignment (6 μm gap, 70 °C) and (b) a cell coated with rubbed polyimide for parallel (homoge-neous) alignment (4 μm gap, 70 °C). Images were taken at crossed polarized conditions and identical magnification. (c) Variable-temperature diffraction patterns of $\mathbf{R12}^{4+}$ as free-standing bulk material. (d) Overlaid images of optical micrographs of a drawn fiber of $\mathbf{R12}^{4+}$ aligned parallel to one of the crossed polarizers and rotated ccw by 45°. (e) 2D-XRD pattern of the drawn fiber at 25 °C; overlaid image of drawn fiber indicates orientation with regard to the detector and orthogonal to the X-ray beam.

The reversible SmX2 to SmA transition at about 13 °C is observed by POM, DSC, and XRD, but the textural changes are small, and both phases are optically uniaxial (see SI). The main differences between the diffraction patterns of the SmX2 and the SmA phases (Figure 3) are a more intense reflection at 15 Å and an additional broad reflection at 4.2 Å for the SmX2 phase. Both reflections are likely caused by a short-range order in the lateral packing of the cores and aliphatic side chains. The observed diffraction patterns resemble those of SmB phases, but the few reflections are insufficient for a definitive assignment, and the large enthalpic change of 32 kJ/mol for the reversible phase transitions between the SmX2 and SmA phases is inconsistent with a SmB to SmA transition.

Diffraction patterns and textures of the SmX1 and SmX2 phases are virtually identical, but the SmX1 to SmA transition occurs at 35 °C higher temperature, and its transition enthalpy is twice as large (see SI). Both, the higher transition enthalpy and temperature are reasoned with a concomitant loss of remaining solvent that could not be removed in high vacuum at room temperature. The loss of solvent is also consistent with the irreversibility of this transition and the assignment as two different phases.

[2]Rotaxane $\mathbf{R16b}^{4+}$ with four-branched 2-hexyl-decyl chains, like its parent dumbbell $\mathbf{D16b}^{4+}$, does not form lamellar mesophases but two different unknown SC phases. *d*-Spacings of their smallest angle reflections are 6−8 Å below the estimated minimum layer spacing of 40 Å for SmA type packing, and the diffraction patterns of both phases contain a large number of weak reflections that indicate a high degree of order, although the broad and intense halos in all XRD patterns of the SC1 and SC2 phases suggest that the side chains are predominantly in an amorphous state (see SI). The SC1 phase is best distinguished from the SC2 phase by the much higher intensity of its reflection at 4.2 Å. DSC measurements show that the SC2 to isotropic liquid transition is reversible on heating but that the isotropic liquid remains stable upon cooling down to −40 °C at scan rates of 5−10 °C/min. The transition from the isotropic phase into the SC2 phase occurs on the subsequent heating run at 124 °C, similar to a cold crystallization.

In summary, attachment of linear aliphatic side chains of 12 or more carbon atoms converts the 4+ charged [2]rotaxanes into smectic liquid crystals, but their smectic phases are still highly viscous and have short-range in-plane order. An increase in length of the aliphatic chains from 12 to 16 carbon atoms stabilizes the SmA phase but generates materials that do not form isotropic liquid phases because of their limited thermal stability. Attachment of branched aliphatic chains in $\mathbf{R16B}^{4+}$ lowers transition temperatures but is not compatible with a lamellar packing of the molecules, most likely because of their increased lateral packing volume.

Mesomorphism: 2+ Charged Materials. Compounds $\mathbf{D12}^{2+}$, $\mathbf{R12}^{2+}$, and $\mathbf{RSi}^{2+}$ based on a 2+ charged design were prepared to generate more fluid and thermally stable mesophases. Dodecane chains were chosen for the 2+ charged compounds $\mathbf{D12}^{2+}$and $\mathbf{R12}^{2+}$ because [2]rotaxane $\mathbf{R12}^{4+}$ showed the most promising phase behavior of the 4+ charged derivatives. Attachment of siloxane chains in $\mathbf{RSi}^{2+}$ was tested as an alternative method to branched aliphatic chains for the lowering of transition temperatures (Figure 9).

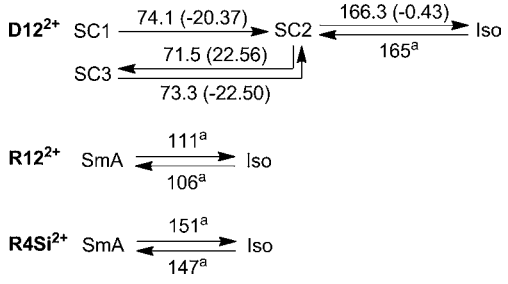

Figure 9. Phase transition temperatures in °C and enthalpies in kJ/mol of 2+ charged dumbbell and [2]rotaxanes based on POM, DSC, and XRD analysis (SC = soft crystal phase ; SmA = smectic A liquid crystal phase; Iso = isotropic liquid phase). (a) Determined by POM.

dx.doi.org/10.1021/ja309558p | J. Am. Chem. Soc. 2013, 135, 400−408

To our surprise dumbbell $\mathbf{D12}^{2+}$ is more crystalline than the 4+ charged dumbbell $\mathbf{D12}^{4+}$ and forms 3 soft-crystal phases SC1 to SC3. The thermal transitions at 70 °C are reversible based on POM and DSC, but XRD patterns of SC1 obtained by precipitation from solution are different than the pattern of SC3 obtained on cooling (see SI). Not fully reversible is the clearing transition at 166 °C as it coincides with the onset of thermal decomposition. A small domain focal conic-type texture is observed by POM, similar to that observed for the mesophases of $\mathbf{D12}^{4+}$, and remains unchanged across the phase transition at 72 °C. What is observed at the phase transition is a softening of the material and a partial melting of the side chains based on XRD, which is consistent with the transition enthalpy of 22 kJ/mol measured by DSC.

In contrast to the results for dumbbells $\mathbf{D12}^{2+}$ and $\mathbf{D12}^{4+}$, the expected increase in fluidity is observed for the SmA phase of [2]rotaxane $\mathbf{R12}^{2+}$ when compared to the SmA phase of $\mathbf{R12}^{4+}$. No transitions are observed by DSC, but POM studies reveal a clearing temperature of 111 °C (see SI). Small domain focal conic defect textures are consistent with a smectic mesophases, and the pseudoisotropic appearance as a free-standing film confirms its optically uniaxial character.

The assignment as a SmA phase is based on the diffraction patterns that consist of only two reflections, an intense small angle peak at a *d*-spacing of about 39 Å and a broad halo at about 4.6 Å that indicates an amorphous state of the side chains (see SI). A second-order reflection of the layer spacing is observed in the diffraction pattern of a free-standing film. Both, POM and XRD results are consistent with the presence of a SmA phase, and this assignment is also supported by the agreement between measured and predicted layer spacings (Table 1). The only change observed in the diffraction patterns with increasing temperature is a small decrease in layer spacing that is common in SmA phases—an increase in layer spacing would be expected for a SmC phase.[27]

Incorporation of siloxane chains in compound $\mathbf{RSi}^{2+}$ was tested because siloxane chains usually lower viscosity and often introduce SmC phases. However, the mesomorphism of $\mathbf{RSi}^{2+}$ is very similar to the mesomorphism of $\mathbf{R12}^{2+}$, although the incorporation of siloxane chains stabilizes the SmA phase by increasing the clearing temperature by 40 to 151 °C (Figures 9 and 10). Again, no transitions are observed by DSC, and the clearing temperature was determined by POM studies. Also consistent with SmA mesomorphism are fan-shaped focal conic textures and a pseudo-isotropic appearance of free-standing films. Diffraction patterns contain an intense small angle peak at a *d*-spacing of 42 Å and two broad halos at about 6.6 and 4.6 Å for the amorphous siloxane and aliphatic side chains, respectively. The observed layer spacing is in good agreement with the estimated value and slightly decreases with temperature as it is common in SmA phases.

In summary, a reduction in charge from 4+ to 2+ for [2]rotaxanes $\mathbf{R12}^{4+}$ and $\mathbf{R12}^{2+}$ lowers transition temperatures and generates a less viscous SmA phase. Exchange of dodecyl by siloxane chains in [2]rotaxane $\mathbf{RSi}^{2+}$ stabilizes the SmA phase compared to $\mathbf{R12}^{2+}$; siloxane chains are more powerful promoters of microphase segregation than aliphatic chains.[16] Although, siloxane chains are known for their high propensity to induce SmC phases, the SmA phase promoting character of ionic liquid crystals appears to be more influential.[9] Disappointing, however, is the low thermal stability of the siloxane chains in these ionic compounds which limits their utility.

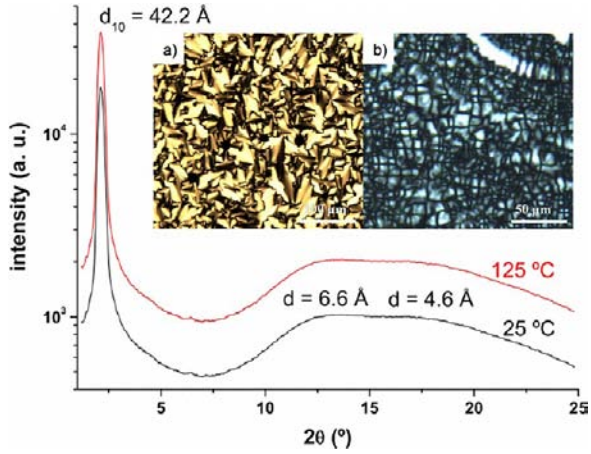

Figure 10. Diffraction patterns of $\mathbf{RSi}^{2+}$ at 125 and 25 °C upon cooling from the isotropic phase. POM photomicrographs of $\mathbf{RSi}^{2+}$ at 25 °C upon cooling from the isotropic phase. (a,b) A fan-shaped focal conic texture is obtained between untreated glass slides and a small domain focal conic texture between cleaned, more hydrophilic, glass slides.

CONCLUSIONS

It has been demonstrated, for the first time, that ionic liquid crystalline [2]rotaxanes based on a small-molecule design can be prepared in gram quantities and good purity by the optimization of design as well as synthetic and purification procedures. Of the two presented designs, the 2+ charged [2]rotaxanes are superior to the 4+ charged [2]rotaxanes because their preparation is less time consuming, they are more easily purified, and they are chemically and thermally more stable. The change from 4+ to 2+ charged [2]rotaxane also improves mesomorphism because (1) the fluidity of the mesophases increases due to the reduction in ionic character and (2) higher temperature phase transitions can be tolerated because of the increased thermal stability.

A comparison of the mesomorphism of dumbbells and [2]rotaxanes provides clear evidence that the interlocked macrocycle promotes the formation of thermotropic ionic liquid crystal phases and increases thermal stability. A reduction in ionic interactions between cores (sheltering of the ions) is proposed as the major reason for the observed change from soft crystal phases for the dumbbells to SmA liquid crystal phases for the [2]rotaxanes. This sheltering of ions is also an advantage of the chosen [2]rotaxane design based on a charged core and a neutral macrocycle, in contrast to the previously reported liquid crystalline [2]rotaxane that consists of a neutral core and a charged macrocycle.

ASSOCIATED CONTENT

Supporting Information

Synthesis of all new compounds and their characterization by ^{1}H and ^{13}C NMR, HR-MS, IR, vt-PXRD, TGA, DSC and POM. SC-XRD analyses of two model compounds with R = CH_3. This material is available free of charge via the Internet at http://pubs.acs.org.

AUTHOR INFORMATION

Corresponding Author

eichhorn@uwindsor.ca; loeb@uwindsor.ca

Notes

The authors declare no competing financial interest.

■ ACKNOWLEDGMENTS

S.J.L. and S.H.E. are grateful for the awarding of NSERC of Canada Discovery grants in support of this research. Additional support was provided to S.J.L. through the NSERC Canada Research Chair program.

■ REFERENCES

(1) (a) Sawamura, M.; Kawai, K.; Matsuo, Y.; Kanic, K.; Kato, T.; Nakamura, E. *Nature* **2002**, *419*, 702. (b) Donnio, B.; Buathong, S.; Bury, I.; Guillon, D. *Chem. Soc. Rev.* **2007**, *36*, 1495.

(2) (a) Kato, T.; Mizoshita, N.; Kishimoto, K. *Angew. Chem., Int. Ed.* **2006**, *45*, 38. (b) Kato, T.; Yasuda, T.; Kamikawa, Y.; Yoshio, M. *Chem. Commun.* **2009**, 729. (c) Nealon, G. L.; Greget, R.; Dominguez, C.; Nagy, Z. T.; Guillon, D.; Gallani, J. L.; Donnio, B. *Beilstein J. Org. Chem.* **2012**, *8*, 349. (d) Rosen, B. M.; Wilson, C. J.; Wilson, D. A.; Peterca, M.; Imam, M. R.; Percec, V. *Chem. Rev.* **2009**, *109*, 6275. (e) Saez, I. M.; Goodby, J. W. In *Liquid Crystalline Functional Assemblies and Their Supramolecular Structures*; Kato, T., Ed.; Springer-Verlag: Berlin, Germany, **2008**; Vol. *128*, p 1. (f) Tschierske, C. *Chem. Soc. Rev.* **2007**, *36*, 1930.

(3) (a) Fahrenbach, A. C.; Bruns, C. J.; Cao, D.; Stoddart, J. F. *Acc. Chem. Res.* **2012**, *45*, 1581. (b) Rambo, Brett M.; Gong, Han-Yuan; Oh, Moonhyun; Sessler, Jonathan L. *Acc. Chem. Res.* **2012**, *45*, 1390. (c) Friscic, T. *Chem. Soc. Rev.* **2012**, *41*, 3493. (d) Beves, J. E.; Blight, B. A.; Campbell, C. J.; Leigh, D. A.; McBurney, R. T. *Angew. Chem., Int. Ed.* **2011**, *50*, 9260. (e) Haenni, K. D.; Leigh, D. A. *Chem. Soc. Rev.* **2010**, *39*, 1240. (f) Gassensmith, J. J.; Baumes, J. M.; Smith, B. D. *Chem. Commun.* **2009**, *42*, 6329. (g) Harada, A.; Hashidzume, A.; Yamaguchi, H.; Takashima, Y. *Chem. Rev.* **2009**, *109*, 5974. (h) Stoddart, J. F. *Chem. Soc. Rev.* **2009**, *38*, 1802. (i) Mullen, K. M.; Beer, P. D. *Chem. Soc. Rev.* **2009**, *38*, 1701. (j) Crowley, J. D.; Goldup, S. M.; Lee, A-L; Leigh, D. A.; McBurney, R. T. *Chem. Soc. Rev.* **2009**, *38*, 1530. (k) Faiz, J. A.; Heitz, V.; Sauvage, J.-P. *Chem. Soc. Rev.* **2009**, *38*, 422. (l) Li, S.; Liu, M.; Zheng, B.; Zhu, K.; Wang, F.; Li, N.; Zhao, X.-L.; Huang, F. *Org. Lett.* **2009**, *11*, 3350. (m) Dichtel, W. R.; Miljanic, O. S.; Zhang, W.; Spruell, J. M.; Patel, K.; Aprahamian, I.; Heath, J. R.; Stoddart, J. F. *Acc. Chem. Res.* **2008**, *41*, 1750. (n) Chmielewski, M. J.; Beer, P. D. Ed.; Atwood, J. L.; Steed, J. W. *Org. Nanostruct.* **2008**, 63. (o) Loeb, S. J. Ed.; Atwood, J. L.; Steed, J. W. *Org. Nanostruct.* **2008**, 33. (p) Champin, B.; Mobian, P.; Sauvage, J.-P. *Chem. Soc. Rev.* **2007**, *36*, 358. (q) Vickers, M. S.; Beer, P. D. *Chem. Soc. Rev.* **2007**, *36*, 211. (r) Saha, S.; Stoddart, J. F. *Chem. Soc. Rev.* **2007**, *36*, 77. (s) Loeb, S. J. *Chem. Commun.* **2005**, 1511. (t) Rowan, S. J.; Cantrill, S. J.; Cousins, G. R. L.; Sanders, J. K. M.; Stoddart, J. F. *Angew. Chem., Int. Ed.* **2002**, *41*, 899. (u) Kim, K. *Chem. Soc. Rev.* **2002**, *31*, 96.

(4) Aprahamian, I.; Yasuda, T.; Ikeda, T.; Saha, S.; Dichtel, W. R.; Isoda, K.; Kato, T.; Stoddart, J. F. *Angew. Chem., Int. Ed.* **2007**, *46*, 4675.

(5) Baranoff, E. D.; Voignier, J.; Yasuda, T.; Heitz, V.; Sauvage, J.-P.; Kato, T. *Angew. Chem., Int. Ed.* **2007**, *46*, 4680.

(6) Kidowaki, M.; Nakajima, T.; Araki, J.; Inomata, A.; Ishibashi, H.; Ito, K. *Macromolecules* **2007**, *40*, 6859.

(7) Yasuda, T.; Tanabe, K.; Tsuji, T.; Coti, K. K.; Aprahamian, I.; Stoddart, J. F.; Kato, T. *Chem. Commun.* **2010**, *46*, 1224.

(8) (a) Roy, D.; Cambre, J. N.; Sumerlin, B. S. *Prog. Polym. Sci.* **2010**, *35*, 278. (b) Stuart, M. A. C.; Huck, W. T. S.; Genzer, J.; Müller, M.; Ober, C.; Stamm, M.; Sukhorukov, G. B.; Szleifer, I.; Tsukruk, V. V.; Urban, M.; Winnik, F.; Zauscher, S.; Luzinov, I.; Minko, S. *Nat. Mater.* **2010**, *9*, 101. (c) Yerushalmi, R.; Scherz, A.; van der Boom, M. E.; Kraatz, H.-B. *J. Mater. Chem.* **2005**, *15*, 4480.

(9) (a) Binnemans, K. *Chem. Rev.* **2005**, *105*, 4148. (b) Axenov, K. V.; Laschat, S. *Materials* **2011**, *4*, 206. (c) Chen, S.; Eichhorn, S. H. *Isr. J. Chem.* **2012**, *52*, 830.

(10) (a) Tabushi, I.; Yamamura, K.; Kominami, K. *J. Am. Chem. Soc.* **1986**, *108*, 6409. (b) Bhowmik, P. K.; Han, S.; Nedeltchev, I. K.; Cebe, J. *J. Mol. Cryst. Liq. Cryst.* **2004**, *419*, 27. (c) Veber, M.; Berruyer, G. *Liq. Cryst.* **2000**, *27*, 671. (d) Wiggins, K. M.; Kerr, R. L.; Chen, Z.; Bielawski, C. W. *J. Mater. Chem.* **2010**, *20*, 5709. (e) Causin, V.; Saielli, G. *J. Mater. Chem.* **2009**, *19*, 9153. (f) Tanabe, K.; Yasuda, T.; Yoshio, M.; Kato, T. *Org. Lett.* **2007**, *9*, 4271.

(11) Veber, M.; Berruyer, G. *Liq. Cryst.* **2000**, *27*, 671.

(12) Wiggins, K. M.; Kerr, R. L.; Chen, Z.; Bielawski, C. W. *J. Mater. Chem.* **2010**, *20*, 5709.

(13) Bruce, D. W. *Acc. Chem. Res.* **2000**, *33*, 831.

(14) (a) Marcos, M.; Ros, M. B.; Serrano, J. L.; Esteruelas, M. A.; Sola, E.; Oro, L. A.; Barbera. *J. Chem. Mater.* **1990**, *2*, 748. (b) Gallardo, H.; Magnago, R.; Bortoluzzi, A. *Liq. Cryst.* **2001**, *28*, 1343.

(15) Kouwer, P. H. J.; Swager, T. M. *J. Am. Chem. Soc.* **2007**, *129*, 14042.

(16) Li, L.; Jones, C. D.; Magolan, J.; Lemieux, R. P. *J. Mater. Chem.* **2007**, *17*, 2313. Roberts, J. C.; Kapernaum, N.; Song, Q.; Nonnenmacher, D.; Ayub, K.; Giesselmann, F.; Lemieux, R. P. *J. Am. Chem. Soc.* **2010**, *132*, 364.

(17) (a) Mercer, D. J.; Vella, S. J.; Guertin, L.; Suhan, N. D.; Tiburcio, J.; Vukotic, V. N.; Wisner, J. A.; Loeb, S. J. *Eur. J. Org. Chem.* **2011**, 1763. (b) Loeb, S. J.; Tiburcio, J.; Vella, S. J.; Wisner, J. A. *Org. Biomol. Chem.* **2006**, *4*, 667. (c) Mercer, D. J.; Yacoub, J.; Zhu, K.; Loeb, S. K.; Loeb, S. J. *Org. Biomol. Chem.* **2012**, *10*, 6094. (d) Mercer, D. J.; Loeb, S. J. *Dalton Trans.* **2011**, *40*, 6386. (e) Davidson, G. J. E.; Loeb, S. J.; Passaniti, P.; Silva, S.; Credi, A. *Chem.—Eur. J.* **2006**, *12*, 3233. (f) Loeb, S. J.; Tramontozzi, D. A. *Org. Biomol. Chem.* **2005**, *3*, 1393. (g) Loeb, S. J.; Wisner, J. A. *Chem. Commun.* **1998**, 2757.

(18) (a) Suzuki, S.; Nakazono, K.; Takata, T. *Org. Lett.* **2010**, *12*, 712. (b) Makita, Y.; Kihara, N.; Takata, T. *J. Org. Chem.* **2008**, *73*, 9245. (c) Makita, Y.; Kihara, N.; Takata, T. *Chem. Lett.* **2007**, *36*, 102. (d) Kawasaki, H.; Kihara, N.; Takata, T. *Chem. Lett.* **1999**, 1015.

(19) (a) Davidson, G. J. E.; Sharma, S.; Loeb, S. J. *Angew. Chem., Int. Ed.* **2010**, *49*, 4938. (b) Loeb, S. J.; Tiburcio, J.; Vella, S. J. *Chem. Commun* **2006**, 1598. (c) Suhan, N. D.; Allen, L.; Gharib, M. T.; Viljoen, E.; Vella, S. J.; Loeb, S. J. *Chem. Commun.* **2011**, *47*, 5991.

(20) (a) Kitaigorodsky, A. I. *Molecular Crystals and Molecules*; Academic Press: New York, 1973. (b) Ubbelohde, A. R. *Melting and Crystal Structure*; Clarendon Press: Oxford, U.K., 1965. (c) Doolittle, A. K. *J. Appl. Phys.* **1951**, *22*, 1471.

(21) Wunderlich, B. *Thermal analysis*; Academic Press: New York, 1990.

(22) (a) Rieger, A. L.; Edwards, J. *J. Org. Chem.* **1988**, *53*, 1481. (b) Farring, J. A.; Ledwith, A.; Stam, M. F. *Chem. Commun.* **1969**, 259. (c) Novakovic, V.; Hoffman, M. Z. *J. Am. Chem. Soc.* **1987**, *109*, 2341.

(23) (a) Neve, F.; Crispini, A.; Armentano, S.; Francescangeli, O. *Chem. Mater.* **1998**, *10*, 1904. (b) Ohta, K.; Sugiyama, T.; Nogami, T. *J. Mater. Chem.* **2000**, *10*, 613. (c) Arkas, M.; Tsiourvas, D.; Paleos, C. M.; Skoulios, A. *Chem.—Eur. J.* **1999**, *5*, 3202. (d) Goossens, K.; Lava, K.; Nockemann, P.; Van Hecke, K.; Van Meervelt, L.; Driesen, K.; Gorller-Walrand, C.; Binnemans, K.; Cardinaels, T. *Chem.—Eur. J.* **2009**, *15*, 656.

(24) (a) Kadam, J.; Faul, C. F. J.; Scherf, U. *Chem. Mater.* **2004**, *16*, 3867. (b) Sorensen, T. J.; Hildebrandt, C. B.; Elm, J.; Andreasen, J. W.; Madsen, A. O.; Westerlund, F.; Laursen, B. W. *J. Mater. Chem.* **2012**, *22*, 4797.

(25) Nguyen, H. T.; Destrade, C.; Malthete, J. In *Handbook of Liquid Crystals*; Demus, D., Goodby, J., Gray, G. W., Spiess, H.-W., Vill, V., Eds.; Wiley-VCH: Weinheim, Germany, 1998; Vol. *2B*, p 865.

(26) Gray, G. W.; Goodby, J. W. *Smectic liquid crystals: Textures and structures*; Heyden & Son: London, 1984.

(27) Dierking, I. *Textures of Liquid Crystals*; Wiley-VCH: Weinheim, Germany, 2003.